Slow Backbone Dynamics of the C-Terminal Fragment of Human Centrin 2 in Complex with a Target Peptide Probed by Cross-Correlated Relaxation in Multiple-Quantum NMR Spectroscopy†

Fatiha Kateb,‡ Daniel Abergel,*,‡ Yves Blouquit,§ Patricia Duchambon,§ Constantin T. Craescu,§ and Geoffrey Bodenhausen‡,||

Département de Chimie, associé au CNRS, Ecole Normale Supérieure, 24 Rue Lhomond, 75231 Paris Cedex 05, France, Institut National de la Santé et de la Recherche Médicale U759 et Institut Curie-Recherche, Centre Universitaire Paris-Sud, Bâtiment 110-112, 91405 Orsay, France, and Institute des sciences et ingénierie chimiques, Ecole Polytechnique Fédérale de Lausanne, EPFL, Batochime, 1015 Lausanne, Switzerland

Received July 20, 2006; Revised Manuscript Received September 13, 2006

ABSTRACT: The C-terminal domain of human centrin 2 (C-HsCen2) strongly binds to P1-XPC, a peptide comprising 17 amino acids with a NWKLLAKGLLIRERLKR sequence. This peptide corresponds to residues N847−R863 of XPC, a protein involved in the recognition of damaged DNA during the initial step of the nucleotide excision repair pathway. The slow internal dynamics of the protein backbone in the C-HsCen−P1-XPC complex was studied by measuring the relaxation rates of zero- and double-quantum coherences involving neighboring pairs of carbonyl ^{13}C and amide ^{15}N nuclei. These relaxation rates, which reflect dynamics on time scales in the range of micro- to milliseconds, vary significantly along the protein backbone. Analysis of the relaxation rates at different $CaCl_2$ concentrations and ionic strengths shows that these slow motions are mainly affected by the binding of a Ca^{2+} ion to the lower-affinity EF-hand III. Moreover, we discuss the possible functional role of residues that undergo differential exchange in the formation of HsCen homodimers.

Calcium ions are involved in many biological processes, ranging from muscle contraction to gene transcription (*1*). Regulation of calcium-mediated cellular signaling depends critically on a class of Ca^{2+} binding proteins, known as the calmodulin (CaM)[1] or EF-hand superfamily. The 29-residue EF-hand motif is composed of a helix−loop−helix scaffold, so folded that it can provide seven ligands (*2*) to the Ca^{2+} ion through main- and side-chain oxygen atoms. Two EF-hand motifs, joined together by an antiparallel β-sheet, form a structural and functional domain, called the EF-hand domain. Centrins are regulatory calcium-binding proteins that constitute a large subgroup of the calmodulin superfamily. Centrins are low-molecular mass (∼20 kDa) biomolecules that are highly conserved in diverse evolutionary eukaryotic lineages from yeast to humans (*3, 4*). The first member of the centrin family was discovered as the major component of striated flagellar rootlets associated with the basal bodies of unicellular green algae (*5*), where it participates in Ca^{2+}-dependent rootlet contractions. Centrins have since been found to be ubiquitous and associated with centrioles of basal bodies and centrosomes, as well as with spindle pole bodies from yeast (*6*). Sequence comparisons of centrins originating from different species revealed that the EF-hand motifs, and particularly the Ca^{2+} binding loops, are the most conserved regions in these proteins. However, some EF-hand motifs among various known isoforms have lost their ability to bind Ca^{2+}. The reasons for the decreased affinity for Ca^{2+} ions are not easy to elucidate. Ca^{2+} binding induces significant conformational changes in EF-hand domains from a compact, closed conformation to an open structure exposing a large hydrophobic surface (*7*). In humans, three centrin isoforms (HsCen1, HsCen2, and HsCen3) with variable levels of sequence identity (53−81%) have been identified, each containing four EF-hand motifs and therefore up to four Ca^{2+} binding sites.

In addition to their role in centriole duplication and dynamics, other functions of centrins in various cell compartments have recently been identified. It was shown that a fraction of HsCen2 that is present in the cell nucleus is involved in the nuclear excision repair (NER) process through its interaction with a major component of the NER system, the XPC−hHR23B heterodimer, composed of the XPC and hHR23B proteins (*8*), thus forming a HsCen2−XPC−hHR23B heterotrimer. NER is a major pathway for recognition and removal of bulky single-strand lesions of

† This work was supported by the Centre National de la Recherche Scientifique, the Institut National de la Santé et de la Recherche Médicale, the Institut Curie, and the Agence Nationale de la Recherche.

* To whom correspondence should be addressed: Département de Chimie, associé au CNRS, Ecole Normale Supérieure, 24 Rue Lhomond, 75231 Paris Cedex 05, France. E-mail: daniel.abergel@ens.fr. Telephone: +33 1 44 32 33 44. Fax: +33 1 44 32 33 97.

‡ Ecole Normale Supérieure.

§ Centre Universitaire Paris-Sud.

|| EPFL.

[1] Abbreviations: CaM, calmodulin; HsCen2, human centrin 2; C-HsCen2, C-terminal domain (residues 94−172) of HsCen2; NER, nucleotide excision repair; XPC, xeroderma pigmentosum group C protein; P1-XPC, peptide with the sequence of 17 amino acids (NWKLLAKGLLIRERLKR) corresponding to residues N847−R863 of XPC.

10.1021/bi061469v CCC: $33.50
Published on Web 11/18/2006

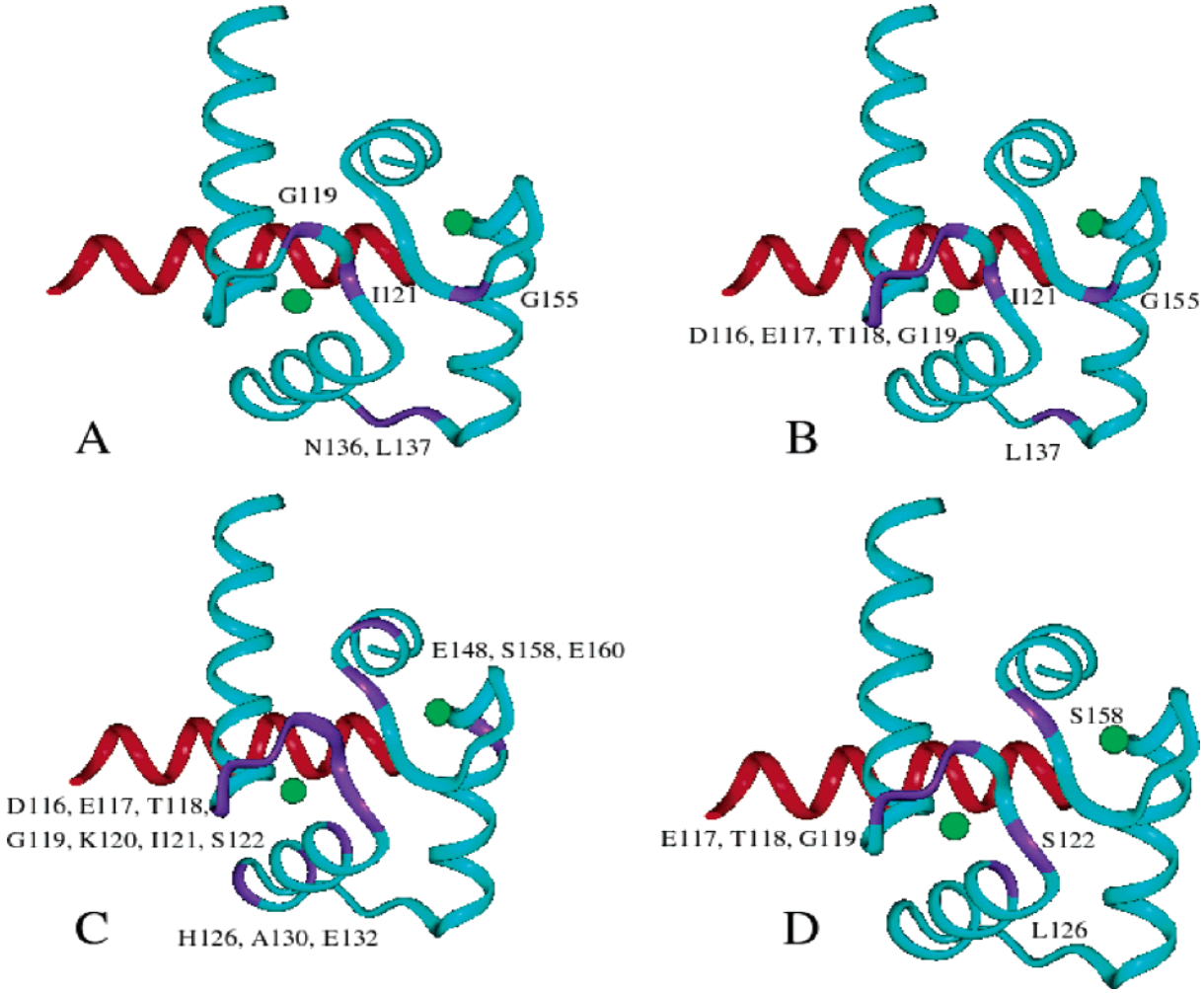

FIGURE 1: Structure of the complex formed by C-HsCen2 (cyan) with P1-XPC (red) (*14*). Calcium ions are shown as green spheres. Residues undergoing conformational exchange contributions significantly larger than those of the rest of the protein are depicted in magenta for (A) 1 mM $CaCl_2$ and (B) 10 mM $CaCl_2$. Residues whose exchange contributions are significantly different at 1 and 10 mM $CaCl_2$ are highlighted in panel C. Panel D shows the residues whose exchange contributions are modified with an increase in the NaCl concentration.

DNA such as UV-induced photoproducts or carcinogenic adducts (*9*). Dysfunction of the NER pathway produces severe disorders, such as the hereditary disease xeroderma pigmentosum, characterized by a high photosensitivity and a 1000-fold increase in the incidence of sunlight-induced skin cancers. Experimental data strongly suggest that the HsCen2−XPC−hHR23B heterotrimer plays a key role in the recognition of damaged DNA during the initial phase of the NER pathway and in the recruitment of key proteins (including transcription factor IIH) involved in damage repair. The association of HsCen2 and the XPC−hHR23B heterodimer stimulates *in vitro* NER activity, by enhancing the specific binding of the HsCen2−XPC−hHR23B heterotrimer to damaged DNA regions (*10*). Recent studies performed on plant cells have confirmed the hypothesis that centrin plays a role in the repair process, by showing that low expression levels of centrin lead to decreased NER activity (*11*).

HsCen2 is a small protein (172 residues, ca. 20 kDa) composed of two EF-hand domains, each of them comprising two EF-hand motifs with variable Ca^{2+} binding affinities. Flow dialysis experiments show that only two Ca^{2+} binding sites have biologically significant affinities, on the order of 10^4 and 10^5 M^{-1} (*12*). Studies on isolated domains demonstrated that these correspond to sites III and IV, respectively (*13*, *14*, *15*). Moreover, we showed that HsCen2 binds the peptide P1-XPC, composed of 17 residues (NWKLLAKGLLIRERLKR) encompassing the sequence of N847−R863 of the XPC protein (*16*). NMR and ITC studies of the interaction between Ca^{2+}-saturated HsCen2 and P1-XPC indicated that binding occurs through the C-terminal domain (C-HsCen2), comprising residues T94−Y172 (*14*, *16*). Previous investigations by NMR spectroscopy demonstrated that the C-terminal domain of HsCen2 acquires a unique stable three-dimensional (3D) structure (see Figure 1) only in the presence of stoichiometric amounts of Ca^{2+} and P1-XPC (*14*). Interestingly, these studies also indicated the presence of slow conformational motions in the loop regions of C-HsCen2 (*14*) that seem to be modulated by the Ca^{2+} concentration.

To characterize motions in the C-HsCen2−P1-XPC−Ca^{2+} ternary complex, we measured not only the relaxation rates of single-quantum coherences SQC(^{15}N) of backbone amide nitrogen nuclei but also the relaxation rates of zero- and double-quantum coherences ZQC(^{13}C,^{15}N) and DQC(^{13}C,^{15}N) of backbone carbonyl and neighboring amide nitrogen nuclei. These rates were studied at two calcium concentrations. Such experiments can reveal motions on fast and slow time scales. The SQC(^{15}N) relaxation rates report mainly on fast subnanosecond motions, while the differences between the ZQC(^{13}C,^{15}N) and DQC(^{13}C,^{15}N) relaxation rates are sensitive to

motions on slow time scales ranging from micro- to milliseconds (*17*−*19*). To our knowledge, this work is the first application of such advanced NMR methods to dynamic effects in a biologically relevant complex. This study may contribute to improving our understanding of the role of centrins in the DNA repair process.

THEORY

It has been shown recently that the relaxation rates of zero- and double-quantum coherences ZQC(^{13}C,^{15}N) and DQC(^{13}C,^{15}N) involving neighboring carbonyl C′ and amide N nuclei in protein backbones can provide evidence of slow motion in proteins (*17*−*19*). Correlated fluctuations involving two dipole−dipole interactions (DD−DD) and two chemical shift anisotropy interactions (CSA−CSA), as well as correlated isotropic chemical shift modulations (CSM−CSM), contribute to the difference ΔR between the relaxation rates of zero- and double-quantum coherences, ZQC($C_{\pm}N_{\mp}$) and DQC($C_{\pm}N_{\pm}$), respectively (*20*−*22*). Thus, the differential line broadening

$$\Delta R = {}^1/_2[R(\mathrm{DQC}) - R(\mathrm{ZQC})] \qquad (1)$$

can be decomposed into a sum of three terms:

$$\Delta R = R^{\mathrm{CSM-CSM}} + R^{\mathrm{DD-DD}} + R^{\mathrm{CSA-CSA}} \qquad (2)$$

The cross-correlated rate $R^{\mathrm{CSM-CSM}}$ accounts for the effect of fluctuations of isotropic chemical shifts, typically on time scales of micro- to milliseconds, that simultaneously affect the environments of C′ and N nuclei belonging to the same peptide plane. These chemical shift changes can be caused either by variations of dihedral angles ϕ and ψ of the backbone, as can be rationalized by ab initio calculations (*23*), or by transient interactions between complexes. In the case of calcium-binding proteins, they can also result from fluctuating interactions with the metal ions. The second term in eq 2 comprises contributions from various auto- and cross-correlated dipole−dipole effects (*20*, *21*). For the worst-case assumption of a rigid backbone, the contributions to $R^{\mathrm{DD-DD}}$ due to dipolar autorelaxation are estimated to be on the order of 0.16 Hz in the C-HsCen2−P1-XPC complex [with an overall correlation time (τ_c) of ∼6 ns] and can therefore safely be neglected. In addition, various cross-correlated dipolar relaxation rates involving external nuclei may contribute to the term $R^{\mathrm{DD-DD}}$. Such dipole−dipole contributions may stem from C′-X/N-X or C′-X/N-Y pairs, where X can be a proton like H^N, H^{α}, etc., and Y a ^{13}C nucleus in the vicinity. Using bond distances derived from the structure of the C-HsCen2−XPC complex [Protein Data Bank (PDB) entry 2A4J], the contribution $R^{\mathrm{DD-DD}}$ in eq 2 can thus be estimated. The third term in eq 2 arises from contributions of cross-correlated CSA relaxation of C′ and N nuclei due to concerted modulations of the chemical shifts that are caused by overall molecular tumbling. An accurate evaluation of these contributions would require the determination of the full CSA tensors of all C′ and N nuclei of C-HsCen2 in the C-HsCen2−P1-XPC complex. However, a recent study of cross-correlated relaxation in ubiquitin (*24*) showed that some of the principal components of the CSA tensors are, to a great extent, independent of the environment, while others are correlated with the isotropic shifts. These empirical correlations were found to be largely independent of the model for the peptide plane motions. Thus, for C′ nuclei in ubiquitin, the σ_{yy} component of the CSA tensor, which is nearly parallel to the C═O bond, turns out to be roughly proportional to the isotropic chemical shift ($\sigma_{yy} = 3\sigma_{\mathrm{iso}} - 334.9$ ppm) while the other two components are almost invariant ($\sigma_{xx} = 251.2$ ppm and $\sigma_{zz} = 83.6$ ppm). For amide ^{15}N nuclei, one finds that $\sigma_{yy} = 2\sigma_{\mathrm{iso}} - 163.2$ ppm, $\sigma_{xx} = \sigma_{\mathrm{iso}} + 105.5$ ppm, and $\sigma_{zz} = 57.7$ ppm. Assuming that these empirical rules, originally derived for ubiquitin (*24*), can also be applied to the C-HsCen2−P1-XPC complex, and using the assignments of the isotropic chemical shifts in this complex, we can estimate the site-specific $R^{\mathrm{CSA-CSA}}$ contributions and hence determine the "corrected" exchange rate $R^{\mathrm{CSM-CSM}}$. This approach is similar to our analysis of cross-correlated relaxation in major urinary protein (MUP) in the presence or absence of a pheromone (*17*).

RESULTS AND DISCUSSION

Overall Molecular Tumbling. Using the strategy developed by Dosset et al. (*25*), no significant anisotropy of rotational diffusion of the C-HsCen2−P1-XPC complex could be determined from R_1(^{15}N) and R_2(^{15}N) measurements. Furthermore, the local correlation times obtained from R_1(^{15}N) and R_2(^{15}N) relaxation rates and from ^{15}N{^{1}H} NOE measurements (*26*, *27*) were found to be nearly constant along the protein backbone. Hydrodynamic calculations (*28*) performed on an ensemble of 20 structures of the C-HsCen2−P1-XPC complex [PDB entry 2A4J (*29*)] yielded three average diffusion coefficients D_x, D_y, and D_z. On the basis of this family of NMR structures, the average ratios and their standard deviations were determined: $D_z/D_y = 0.69 \pm 0.2$ and $D_z/D_x = 0.83 \pm 0.24$. However, due to their large uncertainties, these ratios are not very conclusive. Thus, in the absence of clear evidence of anisotropy, the overall tumbling of the C-HsCen2−P1-XPC complex was assumed to be isotropic. The overall correlation time (τ_c) of the C-HsCen−P1-XPC complex was determined from R_2 and R_1 relaxation rates (*30*, *31*) measured with 100 and 200 mM NaCl, and with a $CaCl_2$ concentration that is either equimolar (1 mM $CaCl_2$) or in excess (10 mM $CaCl_2$) with respect to the C-HsCen−P1-XPC complex. In the sample with 100 mM NaCl and 10 mM $CaCl_2$, an overall correlation time (τ_c) of 6.56 ± 0.07 ns was obtained, whereas with 200 mM NaCl and 10 mM $CaCl_2$, the model-free approach yielded an overall correlation time (τ_c) of 6.01 ± 0.12 ns; with 200 mM NaCl and equimolar 1 mM $CaCl_2$, a somewhat smaller τ_c value of 5.54 ± 0.11 ns was obtained. The larger value obtained in the 100 mM NaCl sample suggests the existence of a monomer−dimer equilibrium, in agreement with previous studies which demonstrated partial dimerization of HsCen2 at lower salt concentrations (*12*, *32*). In addition, the difference in the apparent correlation times obtained in the two samples at 200 mM NaCl may be explained by the existence of slightly different concentrations of the complex. Indeed, in the 1 mM $CaCl_2$ sample, a precipitate was observed upon solvation of the dry mixture of C-HsCen and P1-XPC. This difference in τ_c is therefore likely to arise from the persistence of some small fraction of the complex as a dimer in the sample, even at such a high NaCl concentration.

Model-Free Analysis of Single-Quantum ^{15}N Relaxation. Generalized order parameters [S^2 (*33*)] were obtained for both

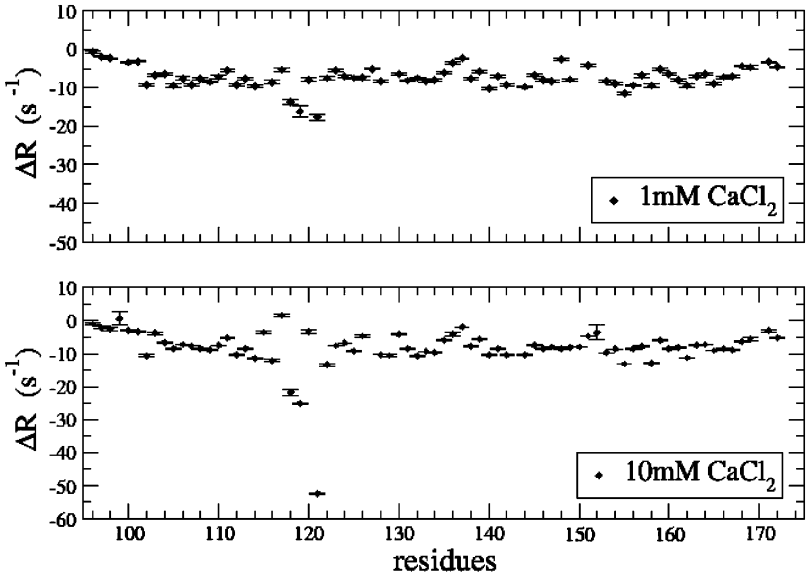

FIGURE 2: Plot of the raw multiple-quantum relaxation rates (ΔR) measured in the C-HsCen−P1-XPC complex in samples with 1 mM $CaCl_2$ (top) or 10 mM $CaCl_2$ (bottom), in 200 mM NaCl in both cases. See the text for details.

NaCl and $CaCl_2$ concentrations (Figure S1 of the Supporting Information). Residues D115, K127, and D150 could not be analyzed due to spectral overlap. In 100 mM NaCl and 10 mM $CaCl_2$, residues E117, L126, N136, and G153 have reduced order parameters. Two residues, E117 and L126, are located in binding loop III, whereas N136 is in the linker domain; G153 belongs to binding loop IV. In 200 mM NaCl and 10 mM $CaCl_2$ (i.e., in excess with respect to the complex), one observes an almost completely flat S^2 profile where, apart from the N-terminal residues, only N136 exhibits significant fast motions. Moreover, for 1 mM $CaCl_2$ (i.e., equimolar with respect to the complex), none of the residues (except for the terminal ones) exhibits any notable mobility. These rather flat S^2 profiles stand in contrast to those obtained for calbindin, another EF-hand protein, where very low order parameters ($0.40 < S^2 < 0.75$) were found for residues located in the linker and its immediate vicinity (*34*).

Exchange contributions (R_{ex}) to the transverse magnetization rates [$R_2(^{15}N)$] were also investigated (Figure S1 of the Supporting Information). In 100 mM NaCl and 10 mM $CaCl_2$, significant R_{ex} contributions were observed for residues E117, T118, and K120, all of which are located in the first binding loop. At 200 mM NaCl with either 1 or 10 mM $CaCl_2$, only residue I121 exhibits any significant exchange effects ($R_{ex} > 2.5\ s^{-1}$). The relaxation rates of I121 with 100 mM NaCl could not be determined because its relaxation was too fast. As slow motions in proteins are often associated with important functional aspects, we undertook a more detailed investigation of movements on the micro- to millisecond time scale in the complex.

Slow Motions Studied by Multiple-Quantum Relaxation Measurements. The slow internal dynamics in the C-HsCen2−P1-XPC complex have been characterized by measuring relaxation rates of zero- and double-quantum coherences involving neighboring pairs of nuclei, $^{13}C'(i-1)$ and $^{15}N(i)$, using a pulse sequence described previously (*17*, *19*). The rates could be measured for almost all peptide bonds in the protein, except for a few residues with overlapping resonances (M97, D115, K127, and D150) or with very fast relaxation (I121, T169, K96, S98, and E99). As explained above, contributions from cross-correlated DD−DD and CSA−CSA effects were estimated from the structure and from the isotropic ^{15}N and ^{13}C chemical shifts of the C-HsCen2−P1-XPC complex.

The influence of the Ca^{2+} concentration on differences in ΔR relaxation rates was investigated for the C-HsCen2−P1-XPC complex in 200 mM NaCl with either 1 or 10 mM $CaCl_2$. Previous work (*13*) showed that the affinity of site IV is ~1 order of magnitude higher than that of site III. This may be explained by the presence of an Asn residue in the highly conserved 12th position of loop III, which, in contrast to the expected Glu, is able to provide only a single oxygen atom from its side-chain carbonyl group for Ca^{2+} binding. Thus, we measured the relaxation rates (ΔR) defined in eq 1 both with 1 mM $CaCl_2$ (equimolar) and 10 mM $CaCl_2$ (i.e., in excess with respect to the C-HsCen2−P1-XPC complex). These ΔR rates are shown in Figure 2. First, the average and standard deviation of all measured rates were calculated. Then, outliers that lie more than 1.5 times the standard deviation from the average were excluded from the average, and a new average and standard deviation were calculated. For an equimolar concentration of 1 mM $CaCl_2$, the resulting set of rates had an average $\langle \Delta R \rangle$ of $-7.32\ s^{-1}$, with a standard deviation σ of $1.82\ s^{-1}$, which represents the dispersion of ΔR about its average along the protein sequence. Similar experiments were performed for the C-HsCen2−P1-XPC with an excess concentration of 10 mM $CaCl_2$. In this case, we obtained a $\langle \Delta R \rangle$ of $-7.48\ s^{-1}$, with a standard deviation σ of $2.99\ s^{-1}$ for a set of 69 residues. As mentioned above, it is possible to estimate the $R^{CSM-CSM}$ relaxation rates by subtracting the calculated DD−DD and CSA−CSA contributions from the relaxation rate ΔR (*24*).

With (equimolar) 1 mM $CaCl_2$ and 200 mM NaCl, one thus finds $\langle R^{CSM-CSM} \rangle = -4.34\ s^{-1}$, with a standard deviation σ_{CSM} of $2.57\ s^{-1}$. This attests to the presence of a significant degree of chemical exchange involving most of the residues in the protein. $R^{CSM-CSM}$ values that significantly differ from

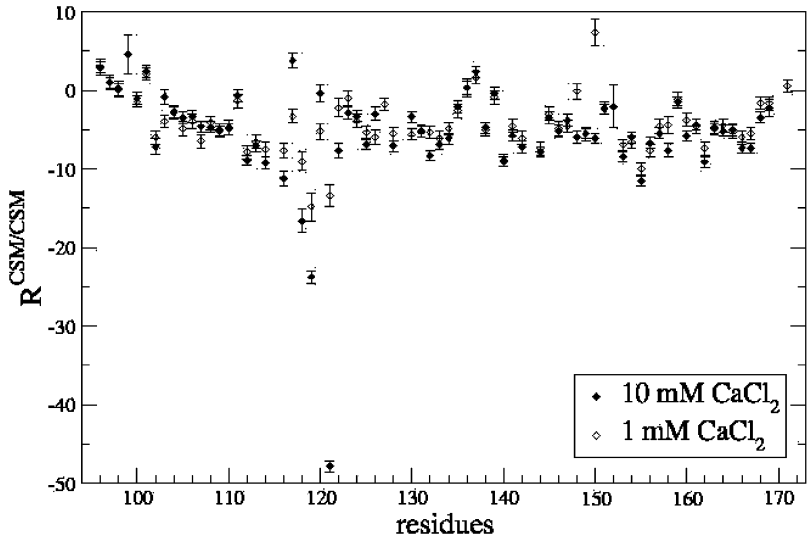

FIGURE 3: Plot of the corrected chemical shift modulation rates ($R^{CSM-CSM}$) measured on the C-HsCen−P1-XPC complex in samples with 1 (◇) and 10 mM $CaCl_2$ (◆), both with 200 mM NaCl. See the text for details.

the average $\langle R^{CSM-CSM} \rangle$ were found for residues G119, I121, N136, L137, and G155, indicating large exchange contributions at these sites. Residues K96, M97, S98, D101, and L171 also have significant exchange contributions. However, these residues are very flexible, since they belong to the N- and C-termini of the protein, so that the calculated dipole−dipole and CSA−CSA contributions to ΔR may not be reliable.

Similarly, in (excess) 10 mM $CaCl_2$, the average $\langle R^{CSM-CSM} \rangle$ was -4.44 s^{-1}, with a standard deviation σ_{CSM} of 3.82 s^{-1}. Rates significantly different from the average were found for only residues D116, E117, T118, G119, I121, L137, and G155. As described above, $R^{CSM-CSM}$ values for residues 96, 99, and 101, which are located in a flexible N-terminal region, could not be considered as reliable evidence for the presence of exchange. These experiments therefore show, for both calcium concentrations, the existence of larger exchange contributions in both EF-hand loops, as well as in the linker region (L137) of the protein in the C-HsCen2−P1-XPC complex.

Slow Motions Are Affected by Protein−Ca^{2+} Interactions. A comparison of $R^{CSM-CSM}$ contributions in the protein at two $CaCl_2$ concentrations may allow one to assess a possible sensitivity of slow motions to the presence of Ca^{2+}. Thus, one finds an average difference of chemical shift modulation rates between samples with 10 and 1 mM $CaCl_2$: $\langle \delta R^{CSM-CSM} \rangle = \langle R^{CSM-CSM}[10] - R^{CSM-CSM}[1] \rangle = -0.54$ s^{-1} with a standard deviation σ_{CSM} of 2.34 s^{-1}. Comparison between both samples allowed identification of residues whose $R^{CSM-CSM}$ contributions were altered by changing the calcium concentration. These are residues D116, E117, T118, G119, K120, I121, S122, N126, A130, E132, E148, S158, and E160. They are mostly located in site III and its vicinity and in loop IV (E148) of the C-terminal domain (Figure 1C). Note that $R^{CSM-CSM}$ rates measured in different samples can be readily compared, despite the difference in τ_c.

Since the $\delta R^{CSM-CSM}$ differences between the two samples with 1 and 10 mM $CaCl_2$ reflect only a change in the line width that is due to exchange, this observation can be interpreted as a modification of exchange upon addition of Ca^{2+}. Moreover, since the magnitudes of the $R^{CSM-CSM}$ rates are larger in the sample with 10 mM $CaCl_2$, this reveals the presence of a significantly increased chemical exchange extending over the first EF-hand motif upon addition of Ca^{2+}, whereas motions in loop IV remain largely unaffected. Because of its lower Ca^{2+} affinity (*14*), binding site III will essentially be loaded only in the presence of a Ca^{2+} excess. Since HsCen2 was shown (*16*) to form a stable complex with P1-XPC and Ca^{2+} at concentrations used in this work, and since the $\delta R^{CSM-CSM}$ differences upon addition of $CaCl_2$ are significant in loop regions only, the increased exchange rates for the corresponding residues must be related to the dynamics of protein−Ca^{2+} interactions.

The multiple-quantum exchange rates were then compared with the R_{ex} exchange contributions obtained by a model-free analysis of single-quantum ^{15}N relaxation measurements. The former are sensitive to correlated chemical shift modulations of $^{13}C'$ and ^{15}N nuclei on the slow micro- to millisecond time scale, which is of particular interest in the case of EF-hand proteins, where backbone C′O groups are involved in metal coordination. In contrast, R_{ex} only probes motions of the $^{15}N-^{1}H$ vectors on the same time scale. Single-quantum $R_2(^{15}N)$ relaxation measurements demonstrate the existence of a relatively small set of residues with significant exchange (see Figure S1 of the Supporting Information). Significant contributions for an R_{ex} of >2.5 s^{-1} to $R_2(^{15}N)$ were found for only residues K120 and I121 in (equimolar) 1 mM $CaCl_2$, and for residues K120, I121, and L127 in (excess) 10 mM $CaCl_2$. In contrast, the multiple-quantum relaxation rate measurements clearly reveal the presence of exchange for a larger number of residues (see Figure 3) for both Ca^{2+} concentrations. These observations therefore demonstrate that multiple-quantum relaxation measurements are sensitive to exchange in the complex. Indeed, it should be remembered that exchange contributions to line widths reflect not only thermodynamic and kinetic parameters (the populations of the exchanging states and the exchange rate constants) but also spectroscopic parameters (the differences between the chemical shifts pertaining to the exchanging states). In principle, these can be separated by multiple refocusing experiments (*35*). Consider the case of a two-site "fast exchange", in the sense that one can observe only a (weighted) average shift, as occurs at temperatures above coalescence. With the

populations p_a and p_b, the contribution R_{ex} to the transverse relaxation rate $R_2(^{15}N)$ in a multiple-echo Carr−Purcell−Meiboom−Gill (*36*, *37*) experiment is (*38*)

$$R_{ex} = \frac{p_a p_b \Delta\omega_N^2}{k_{ex}}\left[1 - \frac{2\tanh(k_{ex}\tau)}{2\tau k_{ex}}\right] \quad (3)$$

where k_{ex} is the exchange rate constant, $\Delta\omega_N$ is the difference between the ^{15}N resonance frequencies in the two exchanging conformations, and 2τ is the time interval between two consecutive 180° refocusing pulses applied to the ^{15}N nuclei in the CPMG sequence. Alternatively, the contribution $R^{CSM-CSM}$ to multiple-quantum relaxation rates that arises from chemical shift modulations in the fast exchange limit is (*39*)

$$R^{CSM-CSM} = \frac{2p_a p_b \Delta\omega_N \Delta\omega_C}{k_{ex}} \quad (4)$$

Thus, for an exchange process with a given kinetic constant k_{ex}, the exchange contributions in eqs 3 and 4 are weighted by different products of chemical shift differences, $\Delta\omega_N^2$ and $\Delta\omega_N\Delta\omega_C$, respectively. Therefore, in our case, observations show that through the effects of the chemical shifts of two distinct nuclei, multiple-quantum relaxation rates ($R^{CSM-CSM}$) appear to be much more sensitive than ^{15}N SQC relaxation to the presence of slow backbone motions. This allowed us to detect exchange contributions in the backbone of the C-HsCen2−P1-XPC complex.

We have shown recently (*14*) that binding of C-HsCen2 to the target peptide P1-XPC in the presence of 1 equivalent of Ca^{2+} considerably increases the structural stability of the protein, which adopts a more stable conformation under these conditions. This is in agreement with the sequence profile of the generalized order parameter S^2 determined in this work, which shows highly restricted fast motions over the major part of the protein. Therefore, the slow motions reported by the $R^{CSM-CSM}$ multiple-quantum relaxation rates pertain to local structural fluctuations, rather than global structural changes, and are clearly localized in the loop fragments involved in Ca^{2+} binding (Figure 1A−C). In addition, $CaCl_2$ titration of the C-HsCen2−P1-XPC complex monitored by ^{15}N HSQC spectra showed that with >1 equivalent of Ca^{2+}, ion binding to the lower-affinity site III appears to affect the dynamic behavior of the complex (*14*). Interestingly, comparison of the $R^{CSM-CSM}$ rates obtained here with 1 and 10 mM $CaCl_2$ (Figure 3) indicates a correlation between the binding of the second metal ion and the modification of slow motions of some residues in site III. One may therefore conclude that the micro- to millisecond motions observed in this work represent local dynamics of loop residues within a stable global scaffold.

The observed Ca^{2+} dependence strongly suggests that this slow conformational exchange is related to the Ca^{2+} off-rate from the low-affinity site. Indeed, from the binding constant determined experimentally, which is on the order of 10^4 M^{-1} (*13*), and assuming a diffusion-controlled on-rate (10^8 M^{-1} s^{-1}), one can calculate an off-rate on the order of 10^4 s^{-1}, which is within the range of time scales of the motions observed here. A similar correlation between Ca^{2+} binding and large-scale slow motions was observed in an artificial CaM variant (*40*).

Finally, the increase in the level of chemical exchange observed in Ca^{2+}-saturated loop IV and its vicinity, as well as in the C-terminal region, where residues do not interact with Ca^{2+} (residues N126, A130, E132, E148, S158, and E160), cannot be ascribed to a direct effect of Ca^{2+}. In this case, the difference in exchange contributions at 1 and 10 mM $CaCl_2$ must be ascribed to a modification of conformational exchange.

Effect of NaCl Concentration. Ca^{2+}-loaded HsCen2, via its C-terminal domain, has a tendency to self-assemble. This tendency decreases with increasing salt concentration (*32*) or in the presence of a tightly bound peptide (*15*). As stated above, the NaCl concentration influences the equilibrium between the dimeric and monomeric forms of the C-HsCen2−P1-XPC complex in solution. The profiles of ΔR relaxation rates measured with (excess) 10 mM $CaCl_2$ are very similar for 100 or 200 mM NaCl, although the rates measured with 100 mM NaCl have a larger magnitude on average ($\langle\Delta R\rangle = -8.88 \pm 3.23$ and $\langle\Delta R\rangle = -7.48 \pm 2.99$ at 100 and 200 mM NaCl; see Figure 4). This difference can be partly ascribed to different apparent correlation times (τ_c) of the C-HsCen2−P1-XPC complex for both NaCl concentrations, most likely due to the presence of complex dimers at 100 mM NaCl (see above).

The difference between the $R^{CSM-CSM}$ rates measured in the 100 and 200 mM NaCl samples was generally small, i.e., $\langle R^{CSM-CSM}[100] - R^{CSM-CSM}[200]\rangle = -0.77$ s^{-1}, with a standard deviation of the difference being 1.43 s^{-1}. It is important to note that for most residues, the $R^{CSM-CSM}$ contributions, which do not depend on the overall correlation time, remain unaffected by the NaCl concentration. Nevertheless, comparison between $R^{CSM-CSM}$ rates observed in both samples reveals significant differences for no fewer than 10 residues (L112, D116, E117, T118, G119, S122, L126, R128, A130, and S158; see Figure 5). These residues are mainly located in calcium binding site III (D116, E117, T118, G119, and S122) and its vicinity (L112, L126, R128, and A130), a region of the protein which is also sensitive to variations of the $CaCl_2$ concentration (Figure 1D).

Calcium affinity of the EF-hand domains is known to depend on the nature and concentration of monovalent ions in solution (*13*, *41*, *42*). The observed changes in $R^{CSM-CSM}$ rates, mainly localized in EF-hand site III, between samples with 100 and 200 mM NaCl seem to indicate that the exchange process is modified in site III through a Na^+-modulated alteration of Ca^{2+} affinity. This conclusion is supported by affinity measurements on the C-terminal domain of centrin (*13*). Moreover, all the residues mentioned above are localized on the same side of the protein. This, together with the fact that residue S158 belongs to high-affinity site IV, whose Ca^{2+} affinity is not Na^+-dependent, may also indicate that these residues belong to the dimerization interface of the complex.

It is interesting to relate these observations to the known tendency of centrins to form oligomers, which depends on several physicochemical parameters: temperature, salt concentration, and pH (*32*). Indeed, although oligomer formation mainly involves the N-terminal domain (*13*, *15*), C-HsCen2 dimers (*12*) were also observed (*13*), which suggests that dimerization can also be mediated by interactions between two C-terminal domains of the integral protein. The monomer−dimer equilibrium shifts toward the monomeric form

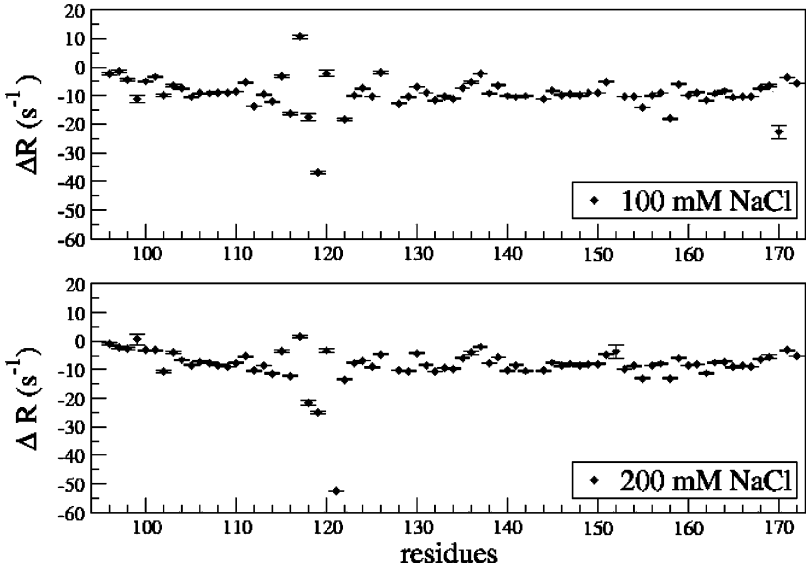

FIGURE 4: Plot of the raw multiple-quantum relaxation rates (ΔR) measured on the C-HsCen−P1-XPC complex in samples with 100 (top) and 200 mM NaCl (bottom). See the text for details.

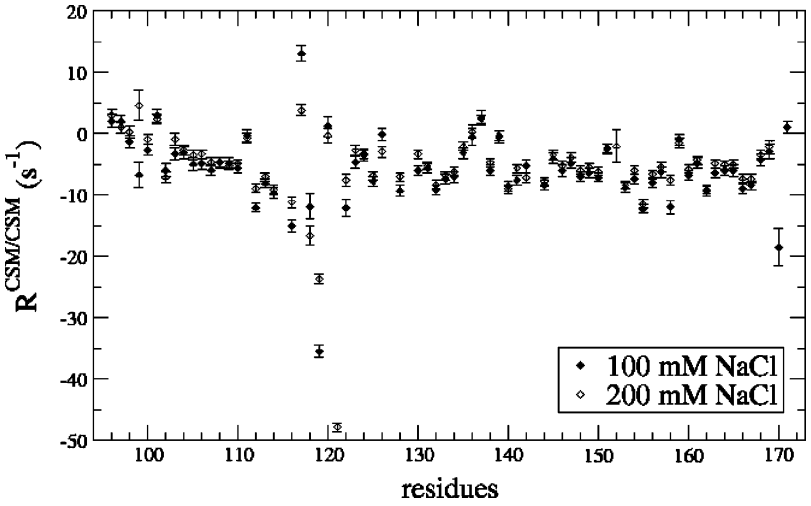

FIGURE 5: Plot of the corrected chemical shift modulation rates ($R^{CSM-CSM}$) measured in the C-HsCen−P1-XPC complex in samples with 100 (◆) and 200 mM NaCl (◇), both with (excess) 10 mM $CaCl_2$.

(*14*) at a high ionic strength (200 mM NaCl) or in the presence of target peptides. The biological significance of the propensity of HsCen2 to form oligomers remains unclear. However, *in vivo*, they are mostly bound to high-affinity targets, forming stable hetero-oligomeric structures, and homomolecular interactions between centrin domains within these complexes could play a role in structural or regulatory functions, as recently suggested in the spindle pole body duplication (*43*).

Comparison of $R^{CSM-CSM}$ Rates with ΔR Measurements. Finally, it is interesting to investigate the possibility to extract information directly from "raw" ΔR measurements, rather than "corrected" $R^{CSM-CSM}$ rates. Note that, at higher fields, both $R^{CSA-CSA}$ and $R^{CSM-CSM}$ terms are expected to increase in proportion to B_0^2, while the perturbation due to R^{DD-DD} does not depend on the static field. Thus, in the sample with equimolar 1 mM $CaCl_2$ and 200 mM NaCl, some residues could be identified which exhibit ΔR rates that are significantly different from the average. As described above, discarding residues K96, M97, S98, K100, D101, and L171, which are located in the N- and C-termini of the protein, we found significant ΔR rates for T118, G119, I121, N136, L137, E148, R151, and G155. Thus, some discrepancies were found between the dynamics identified by ΔR or by $R^{CSM-CSM}$ rates for residues T118, E148, and R151, but their ΔR rates were nearly 1.5σ away from the average. Alternatively, in the sample with (excess) 10 mM $CaCl_2$ and 200 mM NaCl, residues with ΔR rates that differ significantly from $\langle \Delta R \rangle$ (neglecting those located at the protein termini) were found to be E117, T118, G119, I121, S122, L137, G155, and S158. Thus, discrepancies between conclusions drawn from ΔR and $R^{CSM-CSM}$ were found only for residues D116, S122, and S158. If we exclude outliers, the average and standard deviation of the difference of the rates [$\delta\Delta R = \Delta R([CaCl_2]=10\ \text{mM}) - \Delta R([CaCl_2]=1\ \text{mM})$] between the two samples are as follows: $\langle \delta\Delta R \rangle = -0.96\ s^{-1}$ and $\sigma_D = 2.18\ s^{-1}$ (see Figure 2). Residues for which the addition of Ca^{2+} induces a significant difference ($\delta\Delta R$) are E117, T118, G119, I121, and E148. Thus, it is clear from the comparison with the results presented above that analysis of corrected exchange rates ($R^{CSM-CSM}$) affords a much finer picture of the dynamics than a direct analysis of the raw ΔR rates.

Finally, ΔR measurements of samples with different τ_c values cannot be readily compared to retrieve information about the exchange contribution. This problem arises for the C-HsCen2−P1-XPC complex which can be partially dimerized depending on the NaCl concentration. Only after estimation of R^{DD-DD} and $R^{CSA-CSA}$ can such a comparison be made for the corrected $R^{CSM-CSM}$ rates.

CONCLUSIONS

In this study, conformational exchange in the C-HsCen2−P1-XPC complex was investigated using cross-correlated contributions to the relaxation rates of zero- and double-quantum coherences $R_2(C_{\pm}N_{\mp})$ and $R_2(C_{\pm}N_{\pm})$, respectively, involving neighboring backbone carbonyl $^{13}C'$ and amide nitrogen ^{15}N nuclei. This study confirms the potential of this methodology for the study of conformational exchange in proteins. These techniques allowed us to identify sites of conformational exchange, which are mainly located in EF-hand loops. The exchange rates were found to be affected by Ca^{2+} binding and may reflect the high dissociation constant of the metal ion in binding loop III of the protein. In addition, our observations allowed identification of residues that belong to the dimerization interface of the complex, which may help improve our understanding of centrin self-association at the atomic level.

MATERIALS AND METHODS

Sample Preparation. The C-terminal domain (T94−Y172) of HsCen2 was expressed in *Escherichia coli* and purified as described previously (*13*, *16*). Uniform ^{15}N labeling and ^{15}N and ^{13}C labeling were achieved using a minimal medium culture (M9) containing $^{15}NH_4Cl$ and [^{13}C]glucose as the sole source of nitrogen and carbon, respectively. Several samples were obtained by dissolving the lyophilized protein in a buffer containing 20 mM deuterated Tris-DCl, with various NaCl and $CaCl_2$ concentrations. Solutions of 1 mM C-HsCen2 in 100 and 200 mM NaCl and 10 mM Ca^{2+} were prepared. A solution of 1 mM C-HsCen2−P1-XPC complex with 1 mM Ca^{2+} and 200 mM NaCl was also studied. All samples were dissolved in a 93:7 H_2O/D_2O mixture. Unlabeled P1-XPC peptide with the sequence NWKLLAKGLLIRERLKR, which corresponds to the fragment of the human XPC protein (N847−R863) that binds to HsCen2, was purchased from Biofidal (Vaulx-en-Velin, France) and was added in slight molar excess.

NMR Spectroscopy. All experiments were performed at 308 K on a 600 MHz Bruker Avance spectrometer, equipped with triple-axis gradients. Amide $R_1(^{15}N)$ and $R_2(^{15}N)$ relaxation experiments were performed using published pulse sequences (*44*). For $R_1(^{15}N)$ relaxation, nine delays of 5, 50, 100, 150, 250, 300, 370, 500, and 650 ms were used and acquired in an interleaved manner to minimize systematic errors. The recovery delay between acquisitions was 1.8 s, and 16 transients were acquired for each of the 256 t_1 time increments. Water suppression was achieved using the WATERGATE technique (*45*). Single-quantum $R_2(^{15}N)$ relaxation measurements were performed with relaxation periods of 2, 20, 40, 60, 80, 100, 120, and 148 ms, also acquired in an interleaved manner. The recovery delay was 1.8 s; 16 transients were acquired for each of the 256 t_1 increments, leading to a total experimental time of ~27 h. Heteronuclear NOE experiments were performed using eight transients for each t_1 increment, 512 (complex) points in the ^1H dimension, and a recovery delay of 12 s, leading to a total experimental time of ~22 h. The multiple-quantum relaxation experiments were performed using the pulse sequence given in ref *17* (see Figure S2 of the Supporting Information). A single refocusing pulse was used, and coherences $2N_xC_x$ and $2N_yC_y$ were detected in an interleaved manner. To improve the accuracy, the experiment was repeated with three different multiple-quantum relaxation times ($T = 20$, 40, and 50 ms), each obtained with 64 scans, which required ~7 h for each experiment. The R_{MQ} relaxation rates were obtained from the ratio $\langle 2N_xC_x\rangle/\langle 2N_yC_y\rangle = \tanh(\Delta RT)$. All spectra were processed using NMRPipe/NMRDraw (*46*). A squared cosine apodization window was used, and the digital resolution was improved by zero-filling in both dimensions. Peaks were fitted to Gaussian line shapes with the least-squares fitting routine provided.

ACKNOWLEDGMENT

We are indebted to Philippe Pelupessy, Luisa Poggi, Chiara Perazzolo, and Julien Wist for stimulating discussions.

SUPPORTING INFORMATION AVAILABLE

Order parameters (Figure S1) and the pulse sequence used for the measurement of zero- and double-quantum coherence relaxation rates (Figure S2). This material is available free of charge via the Internet at http://pubs.acs.org.

REFERENCES

1. Berridge, M., Bootman, M., and Lipp, P. (1998) Calcium: A life and death signal, *Nature 395*, 645−648.
2. Lewit-Bentley, A., and Réty, S. (2000) EF-hand calcium-binding proteins, *Curr. Opin. Struct. Biol. 10*, 637−643.
3. Schiebel, E., and Bornens, M. (1995) In search for a function for centrins, *Trends Cell Biol. 5*, 197−201.
4. Salisbury, J. L. (1995) Centrins, centrosomes, and mitotic spindle poles, *Curr. Opin. Cell Biol. 7*, 39−45.
5. Salisbury, J. L., Baron, A., Surek, B., and Melkonian, M. (1984) Striated flagellar roots: Isolation and partial characterization of a calcium-modulated contractile organelle, *J. Cell Biol. 99*, 962−970.
6. Wolfrum, U., Giesl, A., and Pulvermüller, A. (2002) Centrins, A Novel Group of Ca^{2+}-Binding Proteins in Vertebrate Photoreceptor Cells, in *Photoreceptors and Calcium*, Baehr, W. and Palczewski, K., Eds. pp 155−178, Kluwer Academic, New York.
7. Ikura, M. (1996) Calcium binding and conformational response in EF-hand proteins, *Trends Biochem. Sci. 21*, 14−17.
8. Araki, M. M., Ushida, A., Sugasawa, K., Kondoh, J., Ohkuma, Y., and Hanaoka, F. (2001) Centrosome protein centrin2/caltractin 1 is is part of the xeroderma pigmentosum group C complex that initiates global genome nucleotide excision repair, *J. Biol. Chem. 276*, 18665−18672.
9. de Laat, W. L., Jaspers, N., and Hoeijmakers, J. (1999) The molecular mechanism of nucleotide excision repair, *Genes Dev. 13* (7), 768−785.
10. Nishi, R., Okuda, Y., Watanabe, E., Mori, T., Iwai, S., Masutani, C., Sugasawa, K., and Hanaoka, F. (2005) Centrin 2 stimulates nucleotide excision repair by interacting with xeroderma pigmentosum group C protein, *Mol. Cell. Biol. 25*, 5664−5674.
11. Molinier, J., Ramos, C., Fritsch, O., and Hohn, B. (2004) Centrin2 modulates homologous recombination and nucleotide excision repair in *Arabidopsis*, *Plant Cell 16*, 1633−1643.
12. Durussel, I., Blouquit, Y., Middendorp, S., Craescu, C. T., and Cox, J. A. (2000) Cation- and peptide-binding properties of human centrin 2, *FEBS Lett. 472*, 208−212.

13. Matei, E., Miron, S., Blouquit, Y., Duchambon, P., Durussel, I., Cox, J. A., and Craescu, C. T. (2003) C-Terminal half of human centrin 2 behaves like a regulatory EF-hand domain, *Biochemistry 42*, 1439−1450.
14. Yang, A., Miron, S., Mouawad, L., Duchambon, P., Blouquit, Y., and Craescu, C. T. (2006) Flexibility and plasticity of human centrin 2 bindingto the xeroderma pigmentosum group C protein (XPC) from nuclear excision repair, *Biochemistry 45*, 3653−3663.
15. Popescu, A., Miron, S., Blouquit, Y., Duchambon, P., Christova, P., and Craescu, C. T. (2003) Xeroderma pigmentosum group c protein possesses a high affinity binding site to human centrin 2 and calmodulin, *J. Biol. Chem. 278*, 40252−40261.
16. Yang, A., Miron, S., Duchambon, P., Assairi, L., Blouquit, Y., and Craescu, C. T. (2006) The N-terminal domain of human centrin 2 has a closed structure, binds calcium with a very low affinity and plays a role in the protein self-assembly, *Biochemistry 45*, 880−889.
17. Perazzolo, C., Wist, J., Loth, K., Poggi, L., Homans, S., and Bodenhausen, G. (2005) Effect of protein-pheromone complexation on correlated chemical shift modulations, *J. Biomol. NMR 33*, 233−242.
18. Wist, J., Perazzolo, C., and Bodenhausen, G. (2005) Slow motions in nondeuterated proteins: Concerted chemical shift modulations of backbone nuclei, *Appl. Magn. Reson. 29*, 251−259.
19. Wist, J., Frueh, D., Tolman, J. L., and Bodenhausen, G. (2004) Triple Quantum Decoherence under Multiple Refocusing Slow Correlated Chemical Shift Modulations of C′ and N nuclei in Proteins, *J. Biomol. NMR 28*, 263−272.
20. Pellecchia, M., Pang, Y. X., Wang, L. C., Kurochkin, A. V., Kumar, A., and Zuiderweg, E. R. P. (1999) Quantitative Measurement of Cross-Correlations between ^{15}N and ^{13}CO Chemical Shift Anisotropy Relaxation Mechanisms by Multiple Quantum NMR, *J. Am. Chem. Soc. 121*, 9165−9170.
21. Konrat, R., and Sterk, H. (1993) Cross-correlation effects in the transverse relaxation of multiple-quantum transitions of heteronuclear spin systems, *Chem. Phys. Lett. 203* (1), 75−80.
22. Frueh, D., Tolman, J. R., Bodenhausen, G., and Zwahlen, C. (2001) Cross-Correlated Chemical Shift Modulation: A Signature of Slow Internal Motions in Proteins, *J. Am. Chem. Soc. 123*, 4810−4816.
23. Arnold, W. D., and Oldfield, E. (2000) The Chemical Nature of Hydrogen Bonding in Proteins via NMR: J-Couplings, Chemical Shifts, and AIM Theory, *J. Am. Chem. Soc. 122*, 12835−12841.
24. Loth, K., Pelupessy, P., and Bodenhausen, G. (2005) Chemical Shift Anisotropy Tensors of Carbonyl, Nitrogen, and Amide Proton Nuclei in Proteins through Cross-Correlated Relaxation in NMR Spectroscopy, *J. Am. Chem. Soc. 127*, 6062−6068.
25. Dosset, P., and Blackledge, M. (2001) *TENSOR2*, Institut de Biologie Structurale J.P. Ebel, CEA-CNRS, Paris, France.
26. Schurr, J. M., Babcock, H. P., and Fujimoto, B. S. (1994) A test of model-free formulas: Effect of anisotropic rotational diffusion and dimerization, *J. Magn. Reson., Ser. B 105*, 211−224.
27. Lee, L. K., Rance, M., Chazin, W. J., and Palmer, A. G. I. (1997) *J. Biomol. NMR 9*, 287−298.
28. Garcia de la Torre, J., Huertas, M. L., and Carrasco, B. (2000) HYDRONMR: Prediction of NMR relaxation of globular proteins from atomic-level structures and hydrodynamic calculations, *J. Magn. Reson. 147*, 138−146.
29. Berman, H. M., Westbrook, J., Feng, Z., Gilliland, G., Bhat, T. N., Weissig, H., Shindyalov, I. N., and Bourne, P. E. (2000) The Protein Data Bank, *Nucleic Acids Res. 28*, 235−242.
30. Kay, L. E., Torchia, D. A., and Bax, A. (1989) Backbone Dynamics of Proteins as Studied by N-15 Inverse Detected Heteronuclear NMR-Spectroscopy: Application to Staphylococcal Nuclease, *Biochemistry 28*, 8972−8979.
31. Clore, G. M., Driscoll, P. C., Wingfield, P. T., and Gronenborn, A. M. (1990) Analysis of backbone dynamics of Interleukin-1β using 2D inverse detected heteronuclear ^{15}N-^{1}H NMR spectroscopy, *Biochemistry 29*, 7387−7401.
32. Tourbez, M., Firanescu, C. A. Y., Unipan, L., Duchambon, P., Blouquit, Y., and Craescu, C. T. (2004) Calcium-dependent self-assembly of human centrin 2, *J. Biol. Chem. 279*, 47672−47680.
33. Lipari, G., and Szabo, A. (1982) Model-Free Approach to the Interpretation of Nuclear Magnetic Resonance Relaxation In Macromolecules 1, Theory and Range of Validity, *J. Am. Chem. Soc. 104*, 4546−4559.
34. Akke, M., Skelton, N. J., Kördel, J., Palmer III, A. G., and Chazin, W. J. (1993) Effects of ion binding on the backbone dynamics of calbindin D9k determined by N-15 NMR relaxation, *Biochemistry 32*, 9832−9844.
35. Palmer, A. G., III, Kroenke, C. D., and Loria, J. P. (2001) Nuclear magnetic resonance methods for quantifying microsecond-to-millisecond motions in biological macromolecules, *Methods Enzymol. 339*, 204−228.
36. Carr, H. Y., and Purcell, E. M. (1954) Effect of diffusion on free precession in nuclear magnetic resonance experiments, *Phys. Rev. 94*, 630−638.
37. Meiboom, S., and Gill, D. (1958) Modified spin-echo method for measuring nuclear relaxation times, *Rev. Sci. Instrum. 29*, 688−691.
38. Allerhand, A., and Thiele, E. (1966) Analysis of Carr-Purcell spin echo experiments on multiple-spin systems. 2. Effect of chemical exchange, *J. Chem. Phys. 45*, 902−916.
39. Frueh, D. (2002) Internal Motions in Proteins and Interference Effects in Nuclear Magnetic Resonance, *Prog. NMR Spectrosc. 41*, 305−324.
40. Evenäs, J., Malmendal, A., and Akke, M. (2001) Dynamics of the transition between open and closed conformations in a calmodulin C-terminal domain mutant, *Structure 9*, 185−195.
41. Linse, S., Helmersson, A., and Forsen, S. (1991) Calcium binding to calmodulin and its globular domains, *J. Biol. Chem. 266*, 8050−8054.
42. Zhu, M. M., Rempel, D. L., Zhao, J., Gibli, D. E., and Gross, M. L. (2003) Probing Ca^{2+}-induced conformational changes in porcine calmodulin by H/D exchange and ESI-MS: Effect of cations and ionic strength, *Biochemistry 42*, 15388−15397.
43. Li, S., Sandercock, A., Conduit, P., Robinson, C., Williams, R., and Kilmartin, J. (2006) Structural role of Sfi1p-centrin filaments in budding yeast spindle pole duplication, *J. Cell Biol. 173*, 867−877.
44. Farrow, N. A., Muhandiram, R., Singer, A. U., Pascal, S. M., Kay, C. M., Gish, G., Shoelson, S. E., Pawson, T., Forman-Kay, J. D., and Kay, L. E. (1994) Backbone Dynamics of a Free and a Phosphopeptide-Complexed Src Homologue Domain Studied by ^{15}N NMR Relaxation, *Biochemistry 33*, 5984−6003.
45. Piotto, M., Saudek, V., and Sklenar, V. (1992) Gradient-Tailored Excitation for Single-Quantum NMR Spectoscopy of Aqueous Solutions, *J. Biomol. NMR 2*, 661−665.
46. Delaglio, F., Grzesiek, S., Vuister, G. W., Zhu, G., Pfeifer, J., and Bax, A. (1995) NMRPipe: A Multidimensional Spectral Processing System Based on UNIX Pipes, *J. Biomol. NMR 6*, 277−293.

BI061469V